ISSN 1674-1056
http://cpb.iphy.ac.cn
http://iopscience.iop.org/cpb
中国物理 B
Chinese Physics
中国物理 Chinese Physics B

Transport spectroscopy through dopant atom array in silicon junctionless nanowire transistors

Xiao-Song Zhao(赵晓松), Wei-Hua Han(韩伟华), Yang-Yan Guo(郭仰岩), Ya-Mei Dou(窦亚梅), Fu-Hua Yang(杨富华)

Citation: Chin. Phys. B . 2018, 27(9): 097310. **doi:** 10.1088/1674-1056/27/9/097310

Journal homepage: http://cpb.iphy.ac.cn; http://iopscience.iop.org/cpb

What follows is a list of articles you may be interested in

Black phosphorus-based field effect transistor devices for Ag ions detection

Hui-De Wang(王慧德), David K Sang, Zhi-Nan Guo(郭志男), Rui Cao(曹睿), Jin-Lai Zhao(赵劲来), Muhammad Najeeb Ullah Shah, Tao-Jian Fan(范涛健), Dian-Yuan Fan(范滇元), Han Zhang(张晗)

Chin. Phys. B . 2018, 27(8): 087308. **doi:** 10.1088/1674-1056/27/8/087308

Electronic transport properties of Co cluster-decorated graphene

Chao-Yi Cai(蔡超逸), Jian-Hao Chen(陈剑豪)

Chin. Phys. B . 2018, 27(6): 067304. **doi:** 10.1088/1674-1056/27/6/067304

Enhanced transient photovoltaic characteristics of core-shell ZnSe/ZnS/L-Cys quantum-dot-sensitized TiO_2 thin-film

Kui-Ying Li(李葵英), Lun Ren(任伦), Tong-De Shen(沈同德)

Chin. Phys. B . 2018, 27(6): 067305. **doi:** 10.1088/1674-1056/27/6/067305

Closed-form internal impedance model and characterization of mixed carbon nanotube bundles for three-dimensional integrated circuits

Qijun Lu(卢启军), Zhangming Zhu(朱樟明), Yintang Yang(杨银堂), Ruixue Ding(丁瑞雪), Yuejin Li(李跃进)

Chin. Phys. B . 2018, 27(1): 017303. **doi:** 10.1088/1674-1056/27/1/017303

Dynamic localization of two electrons in AC-driven triple quantum dots and quantum dot shuttles

Jin-Xian Qu(屈晋先), Su-Qing Duan(段素青), Ning Yang(杨宁)

Chin. Phys. B . 2017, 26(12): 127308. **doi:** 10.1088/1674-1056/26/12/127308

Transport spectroscopy through dopant atom array in silicon junctionless nanowire transistors*

Xiao-Song Zhao(赵晓松)[1,2], Wei-Hua Han(韩伟华)[1,2,†], Yang-Yan Guo(郭仰岩)[1,2], Ya-Mei Dou(窦亚梅)[1,2], and Fu-Hua Yang(杨富华)[1,2,3,‡]

[1] *Engineering Research Center for Semiconductor Integrated Technology, Beijing Engineering Center of Semiconductor Micro-Nano Integrated Technology, Institute of Semiconductors, Chinese Academy of Sciences, Beijing* 100083, *China*

[2] *School of Electronic, Electrical and Communication Engineering, University of Chinese Academy of Sciences, Beijing* 100083, *China*

[3] *State Key Laboratory for Superlattices and Microstructures, Institute of Semiconductors, Chinese Academy of Sciences, Beijing* 100083, *China*

(Received 18 May 2018; revised manuscript received 6 July 2018; published online 28 August 2018)

We demonstrate electron transport spectroscopy through a dopant atom array in n-doped silicon junctionless nanowire transistors within a temperature range from 6 K to 250 K. Several current steps are observed at the initial stage of the transfer curves below 75 K, which result from the electron transport from Hubbard bands to one-dimensional conduction band. The current-off voltages in the transfer curves have a strikingly positive shift below 20 K and a negative shift above 20 K due to the electrostatic screening induced by the ionized dopant atoms. There exists the minimum electron mobility at a critical temperature of 20 K, resulting from the interplay between thermal activation and impurity scattering. Furthermore, electron transport behaviors change from hopping conductance to thermal activation conductance at the temperature of 30 K.

Keywords: ionized dopant atom, junctionless nanowire transistor, hopping, thermal activation, current-off voltage

PACS: 73.63.–b, 81.07.Gf, 85.30.Tv **DOI:** 10.1088/1674-1056/27/9/097310

1. Introduction

During the past few years, much attention has been paid to silicon nanowire transistors which are considered key to future scaling beyond the 10 nm technology node due to their excellent electrostatic control and simple process.[1–4] Moreover, with the shrinking of the device scales, one-dimensional (1D) transport can be clearly observed in silicon nanowire transistors even at room temperature.[5,6] Meanwhile, the influence of dopant atoms is increasingly remarkable on the characteristics of devices in such a small dimension of sub-10 nm. Dopant distribution and fluctuations can cause a device-to-device fluctuation in threshold voltage[7] and on/off current.[8,9] Some work gained a remarkable insight into the transport of electrons in different dopant environments at low or room temperature, such as single dopant atom[10,11] or a few dopant-induced quantum dots.[12–14] Furthermore, when the channel size approaches several tens of nanometers, the electron transport through a dopant-atom array can be observed.[12] The arrangement and position of the dopant atoms have a more significant influence on the transport property in nanowire devices with diameters less than 1 nm.[15,16] It is essential in understanding the influence of the ionized dopant on the electronic characteristic. Here, we explore the transport spectroscopy from Hubbard bands in a dopant atom array to 1D conduction band in n-doped silicon junctionless nanowire transistor (JNT) by varying the temperature from 6 K–250 K. In particular, we study the effect of dopant ionization at critical temperatures on the shifted current-off voltage, the minimum electron mobility, and the transition of electron transport mechanics.

2. Device fabrication

The device fabrication started from a (100)-oriented silicon-on-insulator (SOI) wafer with a top silicon thickness of 55 nm and buried oxide of 145 nm. After growing a 20-nm thermal oxidation layer, the SOI wafer was uniformly implanted by phosphorus ions with a doping fluence of 1×10^{13} cm^{-2} at an energy of 33 keV. A uniform phosphorus doping concentration of $N_D \approx 2 \times 10^{18}$ cm^{-3} could be achieved after annealing at 1000 °C in N_2 for 15 s. Silicon nanowire was defined along the ⟨110⟩ direction by electron beam lithography (EBL) and inductively coupled plasma (ICP) etching. The sacrificial oxidation was introduced to reduce the etching damages. After being rinsed in the 5% HF, the nanowire was oxidized in dry oxygen at 900 °C for 1 h to form a 22-nm gate dielectric and to further reduce the cross-sectional area of the nanowire channel. Finally, a silicon nanowire channel with a width of 18 nm and height of 30 nm was achieved. After depositing a 200-nm-thick polysilicon layer to wrap the nanowires, EBL and ICP etching were used to obtain a polycrystalline silicon gate with a gate length of 280 nm. The

*Project supported by the National Key R&D Program of China (Grant No. 2016YFA0200503) and the National Natural Science Foundation of China (Grant No. 61327813).

†Corresponding author. E-mail: weihua@semi.ac.cn

‡Corresponding author. E-mail: fhyang@semi.ac.cn

© 2018 Chinese Physical Society and IOP Publishing Ltd

top view scanning electron microscopy (SEM) image of our device is shown in Fig. 1(a). After depositing 200-nm SiO_2 for passivation, 20-nm Ni and 300-nm Al were evaporated to form Ni/Si ohmic contact and final metallization with the help of conventional optical lithography. Figure 1(b) shows the schematic structure of our JNT. The single n-channel JNTs were measured in a vacuum chamber at temperatures ranging from 6 K–250 K with the Lakeshore-340 temperature controller and Agilent B1500 semiconductor parameter analyzer.

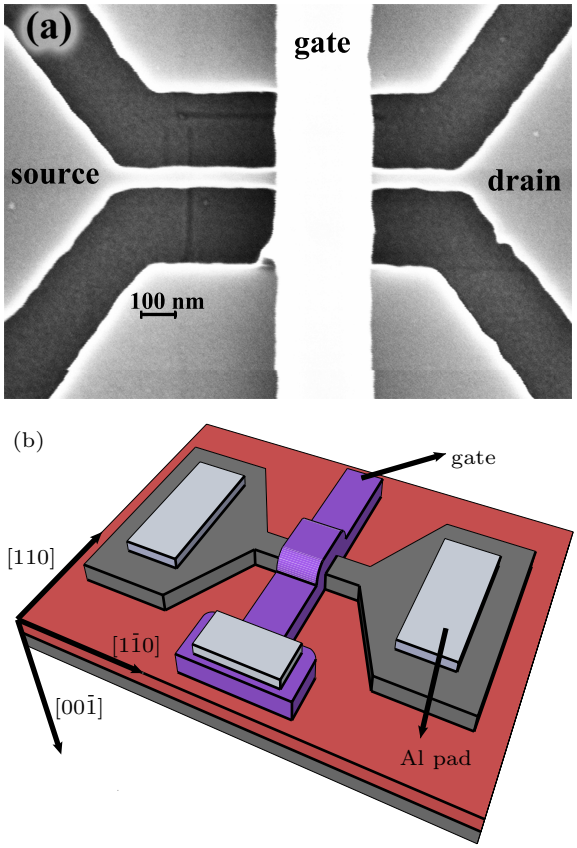


Fig. 1. (color online) (a) Top view SEM image of our device after gate formation. The cross section of channel is 18 nm × 30 nm and the gate length is 280 nm. (b) Three-dimensional schematic of JNT after Al pad formation.

3. Results and discussion

Temperature-dependent transfer characteristics in both linear and log scales are shown in Fig. 2(a) for the JNT at the bias $V_{ds} = 10$ mV within a temperature range from 6 K–100 K. Current steps can be observed clearly below 50 K but gradually smear with the increase of the temperature, and eventually disappear beyond 75 K. The I_{ds}–V_g curves show a current minimum at 20 K for a fixed drain voltage. Moreover, the curves increasing with the temperature rising have a positive shift below a temperature of 20 K and a negative shift above a temperature of 20 K. To show more clearly, the transconductance g_m curves are presented in Fig. 2(b) as a function of gate voltage V_g at $V_{ds} = 10$ mV for various temperatures. The g_m–V_g curve has a maximum positive shift in gate voltage at 20 K, if we set the gate voltage at 6 K as a reference. Each current step in Fig. 2(a) corresponds to the population of an individual 1D sub-band.[17–19] The experimental subband energy spacing can be estimated according to gate voltage spacing ΔV_g from[12,20]

$$\Delta E_{exp} = \frac{\pi\hbar^2 C_{ox}\Delta V_g}{2m^* e}, \tag{1}$$

where m^* is the effective mass of an electron and set to be $0.19m_0$, $\hbar$ is the reduced Planck constant, e is the elementary charge, and C_{ox} is the gate capacitance per unit area and estimated to be 1.56×10^{-7} F/cm^2 for the gate-oxide layer thickness of 22 nm. The values of extracted gate voltage spacing ΔV_g between adjacent transconductance peaks are 1 V, 0.85 V, and 0.91 V at 6 K, respectively, as shown in Fig. 2(b). Correspondingly, the values of energy spacing are estimated to be 6.17 meV, 5.25 meV, and 5.62 meV, which are less than the thermal energy of 6.5 meV at 75 K. Thus, the current steps disappear beyond 75 K where the thermal energy is higher than the subband spacing.

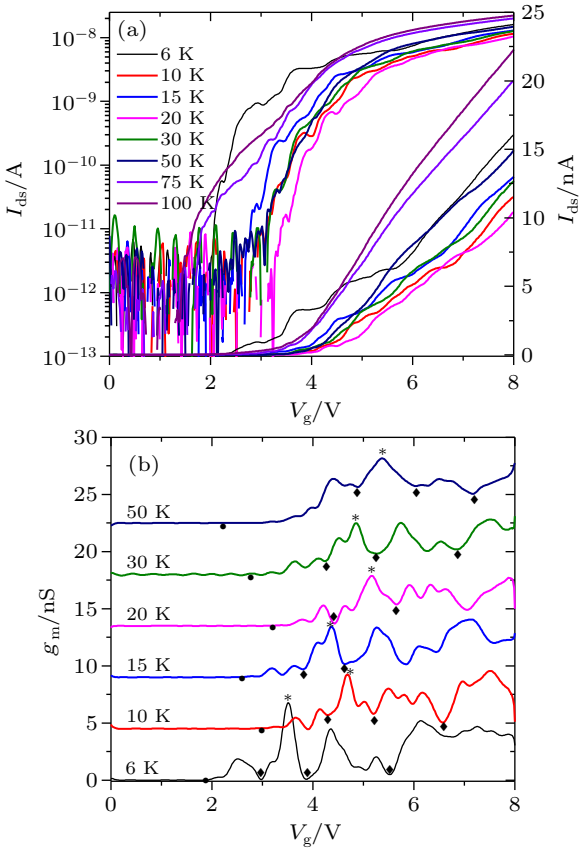


Fig. 2. (color online) (a) Drain current I_{ds} and (b) transconductance g_m ($g_m = \partial I_{ds}/\partial V_{gs}$) versus gate voltage V_g of a single channel JNT at $V_{ds} = 10$ mV at different temperatures. The curves in panel (b) are shifted for clarity.

In order to clarify the effect of temperature on the shift of the curve, the temperature-dependent tendencies of the current-off voltage V_{gp} and the gate voltage V_{gm} at the maximum g_m peak are shown in Fig. 3(a). The current-off voltage V_{gp} is shifted positively from 6 K–20 K and negatively from

20 K–250 K. The gate voltage V_{gm} has a similar temperature-dependent tendency, confirming that the curves varying with temperature have shifted as a whole. To give a clear insight into the inner physics, the temperature dependencies of the effective mobility and electron concentration are drawn in Figs. 3(b) and 3(c), respectively. The effective mobility can be extracted from[21] $\mu_{eff} = g_{m\,max}/C_{ox}(W_{eff}/L)V_{ds}$, where $g_{m\,max}$ is the maximum of transconductance peaks, L is the gate length, and W_{eff} is the effective width and defined as twice the nanowire height plus the nanowire width. A prominent feature shown in Fig. 3(b) is the effective mobility minimum at 20 K. The mobility minimum at 20 K comes from the interplay between impurity scattering and thermal activation at low temperature.[22] As the ionized dopant atoms increase with the temperature rising from 6 K–20 K, more positive scattering centers are induced, resulting in the decrease of the mobility. At higher temperature, the ionized impurity scattering is gradually reduced by the shorter interaction time due to the thermal activation, causing the effective mobility to increase at temperature from 20 K–100 K. Figure 3(c) shows a quantitative result about the electron concentration. The electron concentration from 6 K–250 K can be expressed as[23]

$$n = N_D\left[\frac{F}{2}\left(\sqrt{4+F^2}-F\right)\right], \tag{2}$$

where

$$F = \left(\frac{2N_c}{N_D}\right)^{0.5}\exp(-E_D/2k_BT),\ \ N_c = 2(2\pi m^* k_B T/h^2)^{3/2},$$

N_c is the effective density of states in the conduction band, h is the Planck's constant, and E_D is set to be 2.6 meV according to the minimum effective mobility as discussed in Ref. [22]. The electron concentration is far less than the doping concentration but increases dramatically from 6 K–20 K and tends to be stable at a higher temperature. The increasing of the ionized dopant atoms can be estimated by the electron concentration according to the charge neutrality. The ionized dopant atoms increase dramatically from 6 K–20 K, which accords well with the tendency of the effective mobility. In the silicon nanowire channel, the positive ionized dopant atoms will induce negative charges at the surface of the nanowire[24] which certainly screen the gate voltage to some extent. Larger current-off voltage V_{gp} has to be used to neutralize the electrostatic screening as the ionized dopant atoms increase, resulting in a positive shift of V_{gp} as shown in Fig. 3(a). Above 20 K, the thermally activated electrons increase rapidly to make the current-off voltage V_{gp} decrease, which has been investigated in Refs. [25]–[27]. Therefore, the ionization of the dopant atoms enhances the electron scattering and the electrostatic screening, resulting in the suppression of the effective mobility and the positive shift of the current-off voltage in our JNT.

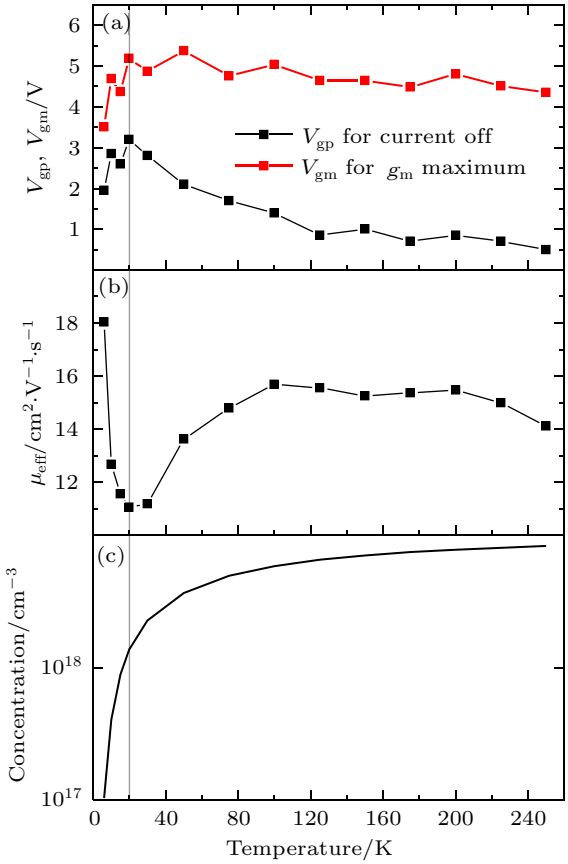


Fig. 3. (color online) (a) The current-off voltage V_{gp} and the gate voltage V_{gm} at the maximum g_m peak versus temperature. The V_{gp} and V_{gm} are marked by dots and asterisks in Fig. 2(b). The current-off voltages are set to be the gate voltage at which the current is 10^{-12} A. (b) Effective mobility dependence on temperature. (c) Electron concentration dependence on temperature.

Figure 4 shows the temperature-dependent evolution of the electron transport spectroscopy from Hubbard bands in a dopant atom array to 1D conduction band. At the initial stage of the conductance below the temperature of 50 K, additional current oscillations before the first current step of 1D transport can be observed at V_{ds} =10 mV as shown in Fig. 4(a). The corresponding transconductance g_m curve is drawn in Fig. 4(b) to clarify the temperature effect of the additional current oscillations. The fine g_m peaks are sensitive to temperature and smear quickly with increasing temperature. At very low temperature, the ionized dopant atoms are isolated and form discrete quantum dots.[28] The three fine g_m peaks at 6 K can be attributed to the transport through three discrete dopant-induced quantum dots.[29] The discrete ionized dopants in an array for the initial channel are coupling with each other to form the Hubbard band due to the repulsion of electrons with the same spin.[30] Two clear g_m envelopes instead of three fine g_m peaks can be observed in Fig. 4(b) from 10 K to 30 K, which validates the formation of the Hubbard band. The two transconductance envelopes are separated by an average gate-voltage spacing $\Delta V_g = 0.464$ V at the temperature range from

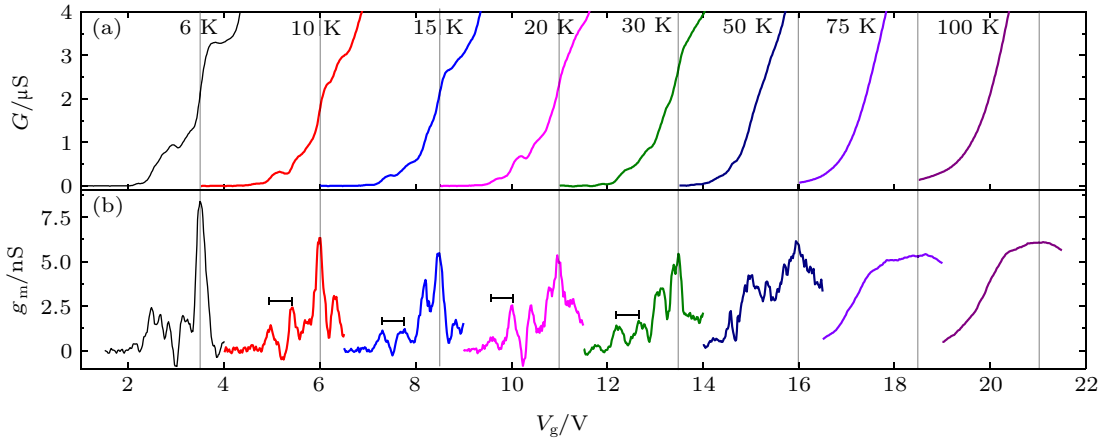


Fig. 4. (color online) (a) Conductance curves G–V_g (a) and (b) transconductance curves g_m–V_g at $V_{ds} = 10$ mV for different temperatures. The curves at each temperature are systematically shifted for the clarity of the fine current steps. The values of gate voltage spacing of two transconductance peaks are 0.464 V at 10 K, 15 K, 30 K and 0.4 V at 20 K, respectively.

10 K to 30 K, corresponding to an energy spacing of 2.85 meV according to Eq. (1). The average energy spacing of 2.85 meV corresponds to the energy gap between two Hubbard bands, which accords well with the value given in Ref. [23] in a similar device. The thermal energy k_BT of electrons at 30 K is about 2.6 meV, which is closer to the calculated energy gap of 2.85 meV. As a result, the merging of two Hubbard bands can be observed at the temperature of 50 K, in which the thermal energy is higher than the Hubbard band gap.

To clarify the electron transport mechanisms at different temperatures, Arrhenius plots of conductance curve at three g_m valleys and the corresponding maximum positions are drawn in Fig. 5(a). The conductances remain stable within the temperature range from 6 K–30 K. The activation energy can be estimated to be 0.14 meV, 0.09 meV, 0.06 meV, and 0.17 meV for the curves at V_{g1}, V_{gm}, V_{g2}, and V_{g3}, respectively, according to the slope of the curve in Fig. 5(a), in which the curve is described by

$$G = G_0 \exp\left(-\frac{E_{act}}{k_BT}\right), \tag{3}$$

where G, E_{act}, and k_B are the conductance, activation energy, and Boltzmann constant, respectively. We conclude that the electrons transport by variable range hopping in local states around the Fermi level.[31] However, the Arrhenius plot of conductance at the temperature of 30 K changes from relatively temperature-independent region to linearly dependent region. The $\ln G$ as a function of $1/T$ has a linear relation in the temperature range from 30 K–100 K. The electron behavior mainly relies on the hopping transport due to the thermal activation. With the temperature increasing, the conductance exponentially increases with the activation energy of 7.54 meV, 4.17 meV, 3.64 meV, and 2.93 meV at the gate voltage V_{g1}, V_{gm}, V_{g2}, and V_{g3}. In Fig. 5(b), the activation energy would decrease and tend to be a constant with the gate voltage increasing, for which the Fermi energy level is driven from the donor band to the conduction band by the gate voltages.

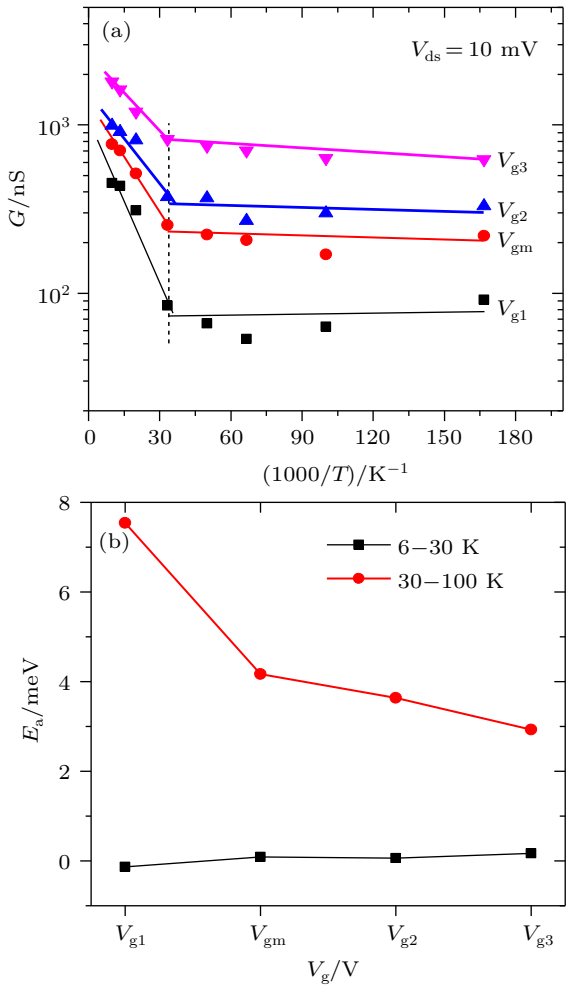


Fig. 5. (color online) (a) Arrhenius plots of conductance at various gate voltages, which correspond to maximum peaks at V_{gm} and three valleys V_{g1}, V_{g2}, V_{g3} in the transconductance curves of Fig. 2(b). (b) Activation energies versus the gate voltage in different temperature regions.

4. Conclusion

In this research, we demonstrate the transport spectroscopy of dopant atom array in heavily n-doped silicon JNT from 6 K–100 K. The clear current steps for 1D subband transport are maintained below the temperature of 75 K. With the temperature increasing form 6 K–20 K, the ionization of the dopant atoms results in the suppression of the effective mobility and the positive shift of the current-off voltage. The transition of the electron transport from the Hubbard band to 1D conduction band is identified below the temperature of 50 K by the temperature-dependent evolution of g_{m} peaks at the initial stage of the transfer characteristics. Arrhenius plots of conductance curves indicate the transition of electron transport mechanism at the temperature of 30 K from relatively temperature-independent region to linearly dependent region. Our study reveals that the ionized dopant atoms play an important role in the performance of silicon JNT. The in-depth understanding of dopant-induced QDs is highly desirable at giving better control for further scaling of transistors.

References

[1] Colinge J P, Lee C W, Afzalian A, Akhavan N D, Yan R, Ferain I, Razavi P, O'Neill B, Blake A, White M, Kelleher A M, McCarthy B and Murphy R 2010 *Nat. Nanotechnol.* **5** 225

[2] Wang B, Zhang H M, Hu H Y, Hu H Y and Shi X W 2018 *Chin. Phys. B* **27** 067402

[3] Liu F Y, Liu H Z, Liu B W and Guo Y F 2016 *Chin. Phys. B* **25** 047305

[4] Nazarov A N and Rudenko T E 2015 *Int. Semiconductor Conf.* **27**

[5] Yi K S, Trivedi K, Floresca H C, Yuk H, Hu W and Kim M J 2011 *Nano Lett.* **11** 5465

[6] Mirza M M, Schupp F J, Mol J A, Maclaren D A, Briggs G A D and Paul D J 2017 *Sci. Rep.* **7** 3004

[7] Shinada T, Okamoto S, Kobayashi T and Ohdomari I 2005 *Nature* **437** 1128

[8] Li Y, Yu S M, Hwang J R and Yang F L 2008 *IEEE Trans. Electron. Devices* **55** 1449

[9] Duan L, Hu F and Ding J W 2011 *Acta Phys. Sin.* **60** 117201 (in Chineses)

[10] Tabe M, Moraru D, Ligowski M, Anwar M, Jablonski R, Ono Y and Mizuno T 2010 *Phys. Rev. Lett.* **105** 016803

[11] Sellier H, Lansbergen G P, Caro J, Rogge S, Collaert N, Ferain I, Jurczak M and Biesemans S 2006 *Phys. Rev. Lett.* **97** 206805

[12] Han W H, Wang H, Yang X, Ma L H, Hong W T, Lyu Q F and Yang F H 2014 *12th International Conference on Solid-State and Integrated Circuit Technology*, October 28–31 2014 Guilin, China, p. 1

[13] Tyszka K, Moraru D, Samanta A, Mizuno T, Jabłoński R and Tabe M 2015 *Appl. Phys. E* **8** 094202

[14] Samanta A, Muruganathan M, Hori M, Ono Y, Mizuta H and Tabe M 2017 *Appl. Phys. Lett.* **110** 093107

[15] Dong J C, Li H, Sun F W, Zhang K and Li Y F 2011 *J. Phys. Chem. C* **115** 13901

[16] Zhang X H, Dong J C, Wang Y, Li L and Li H 2013 *J. Phys. Chem. C* **117** 12958

[17] Guan X M and Yu Z P 2005 *Chin. Phys. Lett.* **22** 2651

[18] Wang H, Han W H, Ma L H, Li X M and Yang F H 2014 *Chin. Phys. B* **23** 088107

[19] Ma L H, Han W H, Wang H, Yang X and Yang F H 2015 *IEEE Electron Device Lett.* **36** 941

[20] Morimoto K, Hirai Y, Yuki K and Morita K 1996 *Jpn. J. Appl. Phys.* **35** 853

[21] Colinge J P, Xiong W, Cleavelin C R, Schulz T, Schrüfer K, Matthews K and Patrunoolinge P 2006 *IEEE Electron Device Lett.* **27** 120

[22] Li X M, Han W H, Wang H, Ma L H, Zhang Y, Du Y D and Yang F H 2013 *Appl. Phys. Lett.* **102** 223507

[23] Ye L X 2012 *Semiconductor Physics* (Vol. 1) (2nd Edn.) (Beijing: Higher Education Press) pp. 118–121 (in Chinese)

[24] Diarra M, Niquet Y M, Delerue C and Allan G 2007 *Phys. Rev. B* **75** 045301

[25] Joo M K, Mouis M, Jeon D Y, Barraud S, Park S J, Kim G T and Ghibaudo G 2014 *Semicond. Sci. Technol.* **29** 045024

[26] de M, Pavanello M A, Trevisoli R D, Doria R T and Colinge J P 2011 *IEEE Electron Device Lett.* **32** 1322

[27] Trevisoli R D, Doria R T, de M and Pavanello M A 2011 *Semicond. Sci. Technol.* **26** 105009

[28] Hong B H, Jung Y C, Rieh J S, Hwang S W, Cho K H, Yeo K H, Suk S D, Yeoh Y Y, Li M, Kim D W, Park D, Oh K S and Lee W S 2009 *IEEE Trans. Nanotechnol.* **8** 713

[29] Ma L H, Han W H, Wang H, Hong W T, Lyu Q F, Yang X and Yang F H 2015 *J. Appl. Phys.* **117** 034505

[30] Mott N F 1968 *Rev. Mod. Phys.* **40** 677

[31] Ye L X 2009 *Semiconductor Physics*, (Vol. 2) (2nd Edn.) (Beijing: Higher Education Press) pp. 540–542 (in Chinese)